Therapeutic targeting of CD146/MCAM reduces bone metastasis in prostate cancer

Eugenio Zoni[1], Letizia Astrologo[1], Charlotte K. Y. Ng[2,3], Salvatore Piscuoglio[3], Janine Melsen[4], Joel Grosjean[1], Irena Klima[1], Lanpeng Chen[5], Ewa B. Snaar-Jagalska[5], Kenneth Flanagan[6], Gabri van der Pluijm[4], Peter Kloen[7], Marco G. Cecchini[$1], Marianna Kruithof-de Julio[1*], George N. Thalmann[8*]

[1]Department for BioMedical Research, Urology Research Laboratory, University of Bern, Bern, CH
[2]Department of Biomedicine, University Hospital Basel, University of Basel, Basel CH
[3]Institute of Pathology, University Hospital Basel, University of Basel, Basel, CH
[4]Department of Urology, Urology Research Laboratory Leiden University Medical Center, Leiden, NL
[5]Institue of Biology, University of Leiden, Leiden, NL
[6]Prothena Biosciences, 331 Oyster Point Blvd, South San Francisco, CA 94080
[7]Department of Orthopedic Trauma Surgery, Academic Medical Center, Amsterdam, NL
[8]Department of Urology, Inselspital, Bern University Hospital, University of Bern, Bern, CH

*Equally Contributed Last Authorship
[$]In memory of Marco G. Cecchini

Running Title: Targeting MCAM reduces bone metastasis in PCa.

Financial Support: This project received support by the Swiss National Science Foundation (310030_156933) and by the Dutch Cancer Society, Grant No. UL2015-7599 KWF. Additional financial support was provided by the Swiss Cancer League (KFS-3995-08-2016 to S.P.) and the Swiss National Science Foundation (Ambizione PZ00P3_168165 to S.P.).

The authors declare no potential conflicts of interest.

Corresponding Authors
Dr. PD Marianna Kruithof-de Julio
Urology Research Laboratory,
Dept. of BioMedical Research, Bern, CH
Phone: +41 31 632 22 59
Fax: +41 31 632 05 51
Email: marianna.kruithofdejulio@dbmr.unibe.ch

and

Prof. George Thalmann
Dept. of Urology
Inselspital, Bern, CH
Phone: +41 31 632 21 84
Email: george.thalmann@insel.ch

Abstract
Prostate Cancer (PCa) is the most common cancer and the second leading cause of cancer-related death in males. When PCa acquires castration resistance, incurable metastases, primarily in the bone, occur. The aim of this study is to test the applicability of targeting MCAM (CD146) with a monoclonal antibody for the treatment of lytic PCa bone metastasis. We evaluated the effect of targeting MCAM using in vivo preclinical bone metastasis models and an in vitro bone niche co-culture system. We utilized FACS, cell proliferation assays, and gene expression profiling to study the phenotype and function of MCAM knockdown in vitro and in vivo. To demonstrate the impact of MCAM targeting and therapeutic applicability, we employed an anti-MCAM monoclonal antibody in vivo. MCAM is elevated in PCa metastases resistant to androgen-ablation. Treatment with Dihydrotestosterone showed MCAM upregulation upon castration. We investigated the function of MCAM in a direct co-culture model of human PCa cells with human osteoblasts and found that there is reduced influence of human osteoblasts on human PCa cells in which MCAM has been knocked down. Furthermore, we observed strongly reduced formation of osteolytic lesions upon bone-inoculation of MCAM-depleted human PCa cells in animal model of PCa bone metastasis. This phenotype is supported by RNA Sequencing analysis. Importantly, in vivo administration of an anti-MCAM human monoclonal antibody reduced tumor growth and lytic lesions. These results highlight the functional role for MCAM in the development of lytic-bone metastasis and suggest that MCAM is a potential therapeutic target in PCa bone metastasis.

Implications:
This study highlights the functional application of an anti-MCAM monoclonal antibody to target prostate cancer bone metastasis.

Introduction

Prostate cancer (PCa) is the most common cancer and the second leading cause cancer-related death in men (1). Current treatments such as radiation therapy and androgen deprivation therapies (ADTs) are effective when the cancer is still confined at the primary site (2). However, after the tumor progresses and acquires castration resistance, the development of incurable metastases is almost inevitable(3).

PCa metastases occur at specific sites with one of the most common locations being the bone, where the occurrence of both lytic- and blastic-lesions has been documented (4). Previous studies demonstrated that PCa cells colonize the bone microenvironment within the so called “hematopoietic stem cell (HSC) niche” (3,5). PCa metastasis initiating cells (MICs) compete with the bone marrow (BM) cells for the occupancy of this microenvironment and induce an ectopic epithelial tissue-of-origin niche, referred as a “developmental prostate niche” (6).

Melanoma Cell Adhesion Molecule (MCAM/CD146) is a cell-surface glycoprotein composed of five immunoglobulin-like domains, one transmembrane region, and a short cytoplasmic tail, which interacts with the cytoskeleton (7). Growing evidence supports the notion that high MCAM expression in a variety of carcinomas positively correlates with poor prognosis in prostate cancer (8), melanoma (9), pulmonary adenocarcinomas (10), epithelial ovarian cancer (11), and breast cancer (12). Overexpression of MCAM has been shown to increase tumorigenicity of human osteoblastic PCa cells (LNCaP) *in vivo* (13). Additionally, MCAM was shown to induce epithelial-to-mesenchymal transition (EMT) in breast cancer, a process thought to be involved in the initiation of metastasis (14).

Upon transplantation, MCAM-expressing subendothelial cells in human BM stroma are capable of recapitulating hematopoiesis in heterotopic sites (15). This established the notion that MCAM-positive subendothelial cells are relevant to hematopoiesis and play key roles in the maintenance of the HSC niche. Previously, we identified a gene signature for the effect that PCa cells exert on the bone stroma in a bone metastasis xenograft mouse model (6). This included MCAM as a potential mediator of the metastatic colonization and growth of PCa cells in the bone in lytic- and blastic-bone metastases (6). The extracellular domain of MCAM can engage in heterophilic binding with various ligands (e.g. Laminin-411). It has also been proposed that homophilic binding with other MCAM molecules (16) might be occurring, suggesting that targeting MCAM on either tumor cells or stromal cells might have a functional effect on PCa cell behavior.

In this study, we show that administration of an anti-MCAM monoclonal antibody reduces intra-osseous growth and lytic lesions in preclinical models of PCa bone metastasis. We provide evidence that MCAM is strongly increased in androgen-ablation resistant metastases derived from PCa and show that MCAM knockdown reduces PCa cell proliferation and osteoblast-mediated induction of ALDH activity. Taken together, these findings suggest that MCAM supports the metastatic lytic-phenotype in human PCa cells and represents a possible therapeutic target in PCa patients with bone metastasis.

Materials and Methods

Cell lines and culture conditions

All the human cell lines employed in this study have been authenticated using highly-polymorphic short tandem repeat loci (STRs). Additionally, all the human cell lines have been previously validated *in vitro* and *in vivo* (17-19). PC-3M-Pro4 were cultured in Dulbecco's modified Eagle's medium (DMEM, GibcoBRL, Waltham, USA) containing 4.5 g glucose/l supplemented with 10% FCII (ThermoScientific, Waltham, USA), 1% Penicillin-Streptomycin (PS, Life Technologies, Carlsbad, USA). PC-3M-Pro4Luc2 and PC-3M-Pro4Luc2dTomato cells were cultured in the same medium supplemented with 0.8 mg/ml Neomycin (Santacruz, Dallas, USA) or Neomycin and 1 µg/ml Blasticidin (Sigma-Aldrich, Zwijndrecht, The Netherlands) respectively. C4-2B cells were cultured in T-medium DMEM (Sigma-Aldrich, St. Louis, Missouri, USA) supplemented with 20% F-12K nutrient mixture Kaighn's modification (GibcoBRL, Waltham, Massachusetts, USA), 10% FCS, 0.125 mg/ml biotin, 1% Insulin-Transferrin-Selenium (ITS), 6.825 ng/ml T3, 12.5 mg/ml adenine, 1% PS. The dTomato clones were supplemented with 1 µg/ml Blasticidin. Osteoblasts were derived and differentiated as we previously described (17). Culture was maintained in DMEM supplemented with 1% PS and 1% ITS. All cells were maintained at 37 ^{o}C and 5% CO_2.

Knockdown of MCAM with shRNA transfection

Short hairpin RNA (shRNA) constructs were obtained from Sigma's MISSION library (MCAM clone# TCRN0000151337 (shRNA#1), TCRN0000155692 (shRNA#2), TCRN0000154854 (shRNA#3)). As a negative control, scrambled shRNA (SHC002, pLKO.1, shRNA-NT) with a lack of homology with any mammalian mRNA sequence was used.

RNA isolation and RT-qPCR

Total RNA was extracted using Trizol (Invitrogen, Waltham, USA) and cDNA synthesized by reverse transcription according to manufacturer's instructions (Promega, Madison, USA). Real-time qPCR was performed with QuantStudio3 system (Thermofisher, Waltham, MA). *ACTIN*, *HPRT* and *GAPDH* housekeeping genes were included for normalization. Primer sequences are reported in **Suppl. Table 1**. Data are displayed as 2^-DCt when Relative Expression is indicated on the "Y" axes.

Western Blot

Anti-vimentin (Ab8979, Abcam, MA, USA) was diluted 1:1000; anti-e-cadherin was diluted 1:1000 (AF648, R&D, Minneapolis, MN, USA); anti-cripto was diluted 1:1000 (clone no. PBL6900 (17)). Detection was performed with 1:10000 secondary horseradish peroxidase (hrp) antibody (NA931VS, NA934VS, Sigma-Aldrich, St. Louis, MO, USA). Actin was detected with 1:20000 hrp antibody (A3854, Sigma-Aldrich).

Flow cytometry, ALDEFLUOR and viable cell sorting

Functional MCAM protein expression was determined by fluorescence-activated cell sorting (FACS) with mouse IgG1 anti-human MCAM-Alexa647 clone P1H12 (BD Biosciences. Franklin Lakes, NJ, USA). Nonspecific binding was excluded by staining with an isotype control antibody (mouse IgG1, BD Biosciences, Franklin Lakes, NJ,

USA). ALDH activity of the tumour cells was measured by the ALDEFLUOR assay kit (StemCell Technologies, Durham, USA) according to the manufacturer's instructions (17). Gating is obtained by acquisition of a control tube for each sample. Therefore, the percentage of $ALDH^{high}$ cells in the control gate correspond always to 0.01% of total. Subsequently the same gate is applied to the sample to assess the percentage of $ALDH^{high}$ cells in each experimental condition. After sorting, samples were controlled to assess purity of the sorted cell populations.

Proliferation assay

Cells were seeded at a density of 1500 cells per well and growth monitored for 24h, 48h, 72h or 96h. For each time point, AU 490nm was measured 2h after incubation with 20 µl of 3-(4,5 dimethylthiazol- 2-yl)- 5 -(3 -carboxymethoxyphenyl)- 2 -(4 -sulfophenyl)- 2 Htetrazolium (MTS - Promega, Madison, Wisconsin, United States) at 37^{o}C according to manufacturer's protocol. Data were normalized for the number of cells seeded. N=5 per condition, performed at least in biological triplicates.

Animal experiments

CB17 SCID male mice, 5-6 weeks old were intra-osseous (IO) injected with 50.000 PC-3M-Pro4Luc2dTomato cells bearing the stable shRNA#1 to knockdown MCAM expression or non-targeted (NT) shRNA control sequence. Sham operated mice were included as additional control (data not shown). Body weight measure, BLI imaging (NightOwl, Berthold, Bad Wildbad, Germany) and x-ray assessment (Faxitron Bioptics, Tucson, Arizona, US), were conducted to monitor the healthy status of the animals, the growth of the tumor cells and the progression of the lesions respectively. Bone morphometry was conducted as described by Bassett et al. (20). A dose of anti-MCAM monoclonal antibody (mAb) 10mg/kg was used (for both the rat anti-mouse and rat anti-human molecule) and animals injected intraperitoneally (i.p.). Same dose was applied to the control IgG molecules. Monoclonal rat IgG1 anti-human MCAM (clone 2107) and rat anti-mouse MCAM mAb (clone 15) were kindly provided by Prothena Biosciences (South San Francisco Ca, USA) (21,22). The anti-human MCAM antibody has previously been tested in 2 clinical trials (ClinicalTrials.gov Identifier: NCT02630901 and NCT02458677). Control IgG (rat Fc and human Fc) were purchased from BioXCell (BE0096 and BE0094, West Lebanon, NH, USA). For zebrafish experiment, Tg(fli1:GFP)i114 zebrafish line (23) was handled according to local animal welfare regulations to standard protocols (http://www.ZFIN.org). Two days postfertilization, dechorionized zebrafish embryos were anesthetized and injected with PC-3M-Pro4Luc2dTomato cells as described previously (17). Data are representative of at least two independent and blind experiments with $\geqslant$30 embryos per group. Survival rate of control group lower than 80% was used as discard cut-off. Images were acquired with Leica SP8 confocal (Leica, Germany).

RNA sequencing

A biological triplicate for MCAM knockdown cells (shRNA#1) and control samples (shRNA-NT) of the cell line employed for the *in vivo* study was generated and total RNA extracted using RNeasy Mini Kit (Qiagen, Venlo, The Netherlands). Samples were measured with NextSeq500 (Illumina, San Diego, US). Image analysis, base calling, and quality check was performed with the Illumina data analysis pipeline RTA v2.4.11 and Bcl2fastq v2.17. Sequence reads were aligned using STAR two-pass (24) to the human reference genome GRCh37 and gene counts quantified using the

'GeneCounts' option. Per-gene counts-per-million (CPM) were computed and log2-transformed adding a pseudo-count of 1 to avoid transforming 0. Genes with log2-CPM <1 in more than 3 samples were removed. Unsupervised clustering was performed using the top 500 most variable genes, Euclidean distance as the distance metric and the Ward clustering algorithm, using the ConsensusClusterPlus (25) R package. Differential expression analysis between MCAM knockdown cells and control samples was performed using the edgeR (26) R package. Normalization was performed using the "TMM" (weighted trimmed mean) method and differential expression was assessed using the quasi-likelihood F-test. Genes with false discovery rate (FDR)<0.05 were considered differentially expressed. Genes differentially expressed by >2-fold were reported. Gene Set Enrichment Analysis (GSEA) was performed using the Preranked tool(27) for the, C2 (canonical pathways) and C5 (biological processes)(28). Genes were ranked based on the F-statistic from the differential expression analysis, multiplying F-statistic of down-regulated genes by -1. Pathways with FDR<0.25 were considered significant. As an alternative, pathway analysis was also performed for the set of differentially expressed genes using g:Profiler(29). Enrichment maps for GSEA and g:Profiler data were generated with Cytoscape(30). Sets of genes with p-value cut-off 0.05 were included and similarity coefficient of 0.5 was applied. The RNA-seq data have been deposited at the NCBI Sequence Read Archive under the accession SRP151808.

Analysis of publicly available dataset for transcriptomic and genomic evaluation and for gene expression-based survival calculation

mRNA data for MCAM expression were extracted with ShinyGEO (31) from the GSE6919 (32,33), GSE6752 (32) and GSE101607 (34) dataset and analyzed with R. Gene expression based survival analysis for MCAM was conducted with PROGgene (35) on GSE40272 (36).

Statistics

Statistical analysis was performed using GraphPad Prism 6.0 (San Diego, CA, USA) using t-test for comparison between two groups or ANOVA for comparison between more groups. Two-way ANOVA was used to examine the influence of knockdown and control cells on the dependent variable (time) in the *in vivo* study. Data are presented as mean±SEM or mean±SD. P-values ≤0.05 are considered to be statistical significant (*p≤0.05, **p<0.01, ***p<0.001).

Study Approval

Animal experiment was approved by the local ethical committee of Canton of Bern, Switzerland (Permit Number BE 55/16) and carried out in accordance with Swiss Guidelines for the Care and Use of Laboratory Animals.

Results

MCAM is highly expressed in PCa and associated metastasis

MCAM expression correlates with poor prognosis in several types of cancer, including PCa (37). We investigated the levels of MCAM in normal (N=18), tumor (N=65) and tumor adjacent tissues (N=63) and PCa metastasis (N=20) in the GSE6919 and GSE6752 datasets (32,33), which include transcriptional data for primary site and androgen-ablation resistant metastases. We found that *MCAM* was increased in tumor (p=0.056) and tumor adjacent tissue (p=0.043) compared to normal samples (**Figure 1A and 1B**). MCAM levels were similar in tumor and tumor adjacent tissues (**Figure 1C**). Moreover, MCAM was strongly increased in PCa metastases (N=20) compared to primary tumors (N=10) (p<0.001 **Figure 1D**). Subsequent fractionation of *MCAM* expression in metastases from various soft tissues (lymph node, adrenal, liver and lung) also revealed a significant increase in *MCAM* expression in these sites compared to the primary tumor site (p=0.001 **Figure 1E**). The relation between *MCAM* expression and PCa recurrence in GSE40272 (36) suggested an involvement of high MCAM expression in disease relapse, although this did not reach significance (**Suppl. Figure 1A and 1B**).

Previously, it was demonstrated that a subpopulation of $ALDH^{high}$ cells isolated from the aggressive PC-3M-Pro4 PCa cell line displays high clonogenicity *in vitro* and possesses the ability to generate bone metastases in preclinical mouse models, compared to non-tumorigenic non-metastatic $ALDH^{low}$ (38). Therefore, we measured the expression of MCAM in selected subpopulations of human PCa cells from the PC-3M-Pro4 cell line and tested whether it was possible to identify a subset of $MCAM^{high}$ cells with aggressive features. Using viable cell sorting, we identified 4 subsets of cells: $ALDH^{high}MCAM^{high}$; $ALDH^{high}MCAM^{low}$; $ALDH^{low}MCAM^{high}$; and $ALDH^{low}MCAM^{low}$ (**Figure 1F** and **Suppl. Figure 1C**). Analysis of MCAM expression by quantitative real-time PCR (RT-qPCR) confirmed that we successfully isolated a subset of $MCAM^{high}$ cells by flow cytometry (**Figure 1G**). However, when tested for colony forming capacity, the 4 subpopulations of cells displayed similar behavior (**Figure 1H and I**).

Characterization of MCAM knockdown cell lines and extravasation ability

We studied the functional role of MCAM in AR-negative and lytic-PCa PC-3M-Pro4 and PC-3M-Pro4 luc2dTomato cells, and in AR-positive and blastic- C4-2B and C4-2BdTomato cells (17).

To investigate the function of MCAM, we used lentiviral delivery of three independent *MCAM*-targeting shRNAs (MCAM KD) and one control non-targeting shRNA (NT). RT-qPCR showed significant reduction of *MCAM* mRNA with each of the 3 *MCAM* shRNAs (shRNA#1; shRNA#2; shRNA#3) compared to the non-targeted control (shRNA-NT) (**Suppl. Figure 2A**). Measurement of functionally active protein by flow cytometry showed marked reduction of MCAM levels with shRNA#1 (approximately 30% reduction vs. NT control cells), whereas similar protein levels were measured for shRNA#2 and shRNA#3 (**Figure 2A**). In C4-2B cells, RT-qPCR displayed strong reduction of *MCAM* mRNA by each of the 3 shRNAs compared to NT control (**Suppl. Figure 2B**). Analysis of functionally active protein expression by flow cytometry showed higher reduction with shRNA#1 and shRNA#3 vs. NT control, compared to shRNA#2 (**Figure 2B**), in line with the transcriptional data.

We found that MCAM knockdown caused a reduction in cell proliferation *in vitro* in PC-3M-Pro4 cells (p<0.01 for shRNA#1 and shRNA#3 at 72 hours and p<0.001 for

shRNA#1 at 96 hours with Bonferroni's multiple comparison test, compared to NT control **Figure 2C**). Similarly, in C4-2B cells, MCAM knockdown reduced proliferation *in vitro* ($p<0.001$ for shRNA#1, shRNA#2 and shRNA#3 at 72 hours and $p<0.001$ for shRNA#3 at 96 hours with Bonferroni's multiple comparison test **Figure 2D**). Based on these results and on the knockdown validation at the protein level, we selected the shRNA#1 to continue with subsequent *in vitro* and *in vivo* characterization.

To assess the role of MCAM in the modulation of ALDH activity in PC-3M-Pro4 cells we employed the ALDEFLUOR assay (**Figure 2E**). MCAM knockdown cells displayed a lower percentage of $ALDH^{high}$ cells compared to NT control, although this did not reach statistical significance (**Figure 2F**). Similarly, no change was observed in C4-2B PCa cells (**Figures 2G and 2H**). This suggests that knockdown of MCAM does not cause depletion of the $ALDH^{high}$ population of human PCa cells. Analysis of a panel of EMT markers (*E-Cad, N-Cad, Vim, Zeb1, Zeb2, Snail1, Snail2* and *Twist*) in the presence or absence of MCAM knockdown suggests that suppressing MCAM expression promotes an epithelial transcriptional phenotype as shown by the significant increase in the ratio E-Cad/Vim in both cell lines ($p<0.001$ for PC-3M-Pro4 and $p<0.01$ for C4-2B **Figure 3A and 3B**) and by the increase in the ratio E-Cad/N-Cad in PC-3M-Pro4 ($p<0.001$ **Suppl. Figure 2C-D-E**). However, evaluation of protein expression by western blot revealed a non-significant alteration in E-Cadherin and Vimentin expression (**Figure 3C-D-E and 3F**– left panel) and in the ratio E-Cad/Vim **(Figure 3F** – right panel). We used zebrafish to assess the impact of MCAM knockdown on the ability of PCa cells to extravasate, which is an EMT feature, and to grow at distant sites (**Suppl. Figure 2F**). Quantification of disseminated cells at 1 day post injection (dpi) and 4 dpi revealed similar behavior in knockdown and control (**Suppl. Figure 2G**), supporting our analysis on E-Cadherin and Vimentin expression.

MCAM is required for osteoblast-mediated induction of ALDH activity in PCa cells and is increased upon castration

The osteoblastic microenvironment in bone functions as premetastatic niche by attracting bone-metastasizing PCa cells (5). We have previously shown that co-culture of human PCa cells and mature human osteoblasts leads to increase in the percentage of highly metastatic $ALDH^{high}$ PCa cells (17).

To investigate the role of MCAM in the context of the osteoblastic niche, we performed direct co-culture of MCAM knockdown PCa cells and human osteoblasts. After 48 hours of co-culture, the dTomato labelled PC-3M-Pro4 PCa cells were separated from the osteoblasts by viable cell sorting (**Figure 3G**). Immediately after sorting, we measured the ALDH activity of the sorted PC-3M-Pro4 MCAM knockdown (ShRNA#1) and control PCa cells (Sh-NT) that were either co-cultured (Sh-NT+OB; ShRNA#1+OB **Figure 3H**. Each condition includes its own gating control, small insert in each panel) or not co-cultured (Sh-NT-OB; ShRNA#1-OB **Figure 3H**) with osteoblasts. In the absence of osteoblast co-culture, NT and MCAM knockdown cells each displayed similar percentages of $ALDH^{high}$ cells (**Figure 3I** – CTRL bars). However, when co-cultured with osteoblasts, the MCAM knockdown PCa cells displayed a significant reduction in the percentage of $ALDH^{high}$ cells - when compared to NT PCa cells co-cultured with osteoblasts ($p<0.01$ **Figure 3I** – OB bars). This result indicates that MCAM plays a role in maintaining levels of ALDH activity in PCa cells in the presence of osteoblast cells in co-culture and suggests that it may play a similar role within the osteoblastic microenvironment. To test if there is cross-talk between MCAM and the androgen signaling in the context of PCa bone metastasis, we evaluated the expression level of MCAM and its extracellular matrix interaction

partner laminin alpha 4 (LAMA4) in the GSE101607 dataset (34), which contains fresh-frozen bone metastasis samples from AR driven (N = 32) and non-AR driven (N = 8) tumors. We found a significant increase in MCAM (p=0.044) and LAMA4 (p=0.045) in non-AR-driven conditions compared to AR-driven (**Figure 4A and 4B**). This reinforces the hypothesis that MCAM levels increase upon disease progression. Furthermore, we evaluated the effect of DHT administration in C4-2B cells under high-castration conditions in Charcoal Stripped Medium for 72 hours (39) (**Figure 4C**). The androgen response was compared in control and MCAM knockdown cells by evaluating the expression of 4 androgen responsive genes upon DHT stimulation (10nM) (40). C4-2B cells displayed an intact AR machinery as indicated by the strong upregulation of FKBP5, KLK3 and TMPRSS2 and by the downregulation of OPRK1 (**Figure 4D**) (40). No difference was detected between control and knockdown cells, indicating that MCAM has no influence on the androgen responsiveness in C4-2B cells. Similarly, administration of the anti-androgen MDV3100 (Enzalutamide) revealed no difference in the modulation of the AR responsive genes in control and knockdown cells (**Figure 4E**). Interestingly, we observed a consistent downregulation of OPRK1 in MCAM knockdown cells compared to control. Finally, while no change was observed on MCAM expression upon MDV3100 treatment compared to DMSO control, DHT administration resulted in a strong reduction of MCAM expression compared to castration (EtOH control in Charcoal Stripped Medium) (**Figure 4F**). This supports our dataset analysis and indicates that MCAM levels are higher upon castration.

MCAM knockdown reduces PCa lytic bone metastasis in a preclinical mouse model

To test the impact of MCAM knockdown on bone metastasis of PCa cells, we performed intra-osseous (IO) inoculation of PC-3M-Pro4 MCAM knockdown cells and NT control cells expressing Luciferase2 (Luc2) in male mice (sham-operated mice were included as an additional control). Animals were monitored by bioluminescent imaging (BLI) during the course of the experiment (4 weeks, **Figure 5A.** All animals, at day 7 and day 28 displayed in **Suppl. Figure 3A**). Luciferase activity of MCAM knockdown and NT control cells was assessed by serial cell dilution to confirm that there was no external influence of the shRNAs employed on BLI signal detection (**Suppl. Figure 3B**). Body weight of the animals was monitored along the course of the experiment (**Suppl. Figure 3C**) and the development of bone lesions was assessed by X-Ray measurements (**Figure 5B**. Data for all mice, including sham, at day 7 and day 28 are displayed in **Suppl. Figure 3D**). We found that MCAM knockdown strongly reduced the lytic-phenotype of PC-3M-Pro4 cells compared to NT control. This was confirmed by bone morphometric analysis (**Figure 5C** and **Suppl. Figure 3E**, analysis at day 28) and histological evaluation (**Figure 5D** and **Suppl. Figure 3F**). Bone morphometry revealed that bone area in knockdown was similar to sham and significantly higher in mice injected with MCAM knockdown cells compared with those injected with NT control cells ($p<0.05$ **Figure 5E**) despite the fact that BLI measurement revealed similar tumor burden between MCAM knockdown and NT control cells (**Figure 5F**). Finally, we used RT-qPCR to measure the expression of a panel of genes previously identified as regulators of multiple steps of the bone metastatic cascade (TDGF1/CRIPTO, PMEPA1, COL1a, VEGFa, DKK1, PTHLH, MSF) (17,41). We found a strong inhibition of the oncogene

CRIPTO/TDGF1 (42) in MCAM knockdown cells compared to NT control ($p<0.05$) and a general modulation of molecules involved in bone remodeling (e.g. PTHLH and DKK1 **Figure 5G**). The downmodulation of CRIPTO/TDGF1 in MCAM knockdown cells was confirmed also at protein level (**Figure 5H**). Taken together, our data suggest that MCAM influences the expression of molecules that are important modulators of bone remodeling and bone metastasis.

MCAM knockdown impacts expression of genes that regulate hematopoiesis and bone remodeling

To identify the putative mechanisms of action of MCAM, we performed RNA-sequencing on MCAM knockdown cells. Unsupervised hierarchical clustering demonstrated a separation between MCAM knockdown and control NT samples (**Figure 6A**, heatmap and volcano plot in upper and lower panel, respectively). Differential expression analysis between MCAM knockdown and NT control revealed that 55 different genes were significantly upregulated (> 2 fold increase, FDR < 0.05) and 99 significantly downregulated (> 2 fold decrease, FDR < 0.05) (**Suppl. Table II** and **Suppl. Table III**). We performed gene set enrichment analysis (GSEA)(27) to identify biological processes and pathways modulated by MCAM knockdown (**Figure 6B**). We found that the upregulated genes in MCAM knockdown cells were enriched for the process related to negative regulation of hematopoiesis (normalized enrichment score (NES)=1.68, p=0.02, **Figures 6C and Suppl. Table IV** for the list of 14 genes involved in the pathway). This supports our previous findings (6) and the notion that increasing the number of HSC niches increases metastatic growth in the bone marrow (5). Additionally, we found an enrichment of GO processes of biomineral tissue development (NES=1.8, p=0.002) and bone mineralization (NES=1.68, p=0.008) among the genes upregulated upon MCAM knockdown (**Figures 6D, 6E and 6F**). This support the hypothesis that MCAM knockdown disrupts signaling pathways associated to bone remodeling and are in accordance with our *in vivo* experiment.

Among the genes downregulated in MCAM knockdown cells, we found an enrichment of genes involved in G0 and early G1 (NES = -1.5, p=0.02) and in E2F mediated regulation of DNA replication (NES = -1.5, p=0.01) **(Suppl. Figure 4A and B** and **Suppl. Table V and VI).** These data reinforce our finding that MCAM knockdown cells displayed reduced proliferation *in vitro*. Similar results were obtained using an alternative gene set analysis method g:Profiler (**Suppl. Figures 4C and D**).

Targeting MCAM with a monoclonal antibody reduces intra-osseous growth and diminishes the extension of lytic-lesions in an intra-osseous model

To test the effect of targeting MCAM on both the tumor and the stroma in a preclinical intra-osseous model of PCa bone metastasis, we employed an anti-human and anti-mouse MCAM mAb. Five animals per experimental group (anti-human, anti-mouse, anti-human+mouse, control IgG rat, control IgG human) were pre-treated with 10mg/kg of mAbs and controls IgG intraperitoneally the day prior to intra-bone injection of PCa cells. After intra-bone injection, all animals received administration of the mAbs or controls IgG every second day at a dose of 10mg/kg intraperitoneally. Animals were monitored by BLI during the course of the experiment (5 weeks, **Figure 7A**, all animals at end of experiment displayed in **Suppl. Figure 5A**). Administration

of anti-human MCAM mAb resulted in significantly smaller intra-osseous growth ($p<0.05$ **Figure 7B**). Body weight was evaluated, and development of bone lesions was monitored during the experiment with x-ray (**Figure 7C** and **7D**, all animals displayed in **Suppl. Figure 5B** and statistic in **Suppl. Figure 5C**). Additionally, luciferase activity of PCa cells was evaluated prior to *in vivo* experimentation (**Suppl. Figure 5D**). Bone morphometric analysis and histological evaluation revealed a higher bone area in animals treated with anti-human mAbs compared to other experimental groups ($p<0.05$, **Figure 7E** and **7F**, all animals displayed in **Suppl. Figure 6A-D**. Statistical evaluation displayed in **Suppl. Figure 6B** and **C**). Evaluation of the kidney histology revealed normal and comparable histological characteristics in all the experimental groups (**Suppl. Figure 7A**). Contralateral bones as control of normal histological features were collected and displayed in **Suppl. Figure 7B**.

Discussion

In this study we provide evidence that MCAM drives lytic-metastatic human PCa and has potential as a therapeutic target in metastatic PCa.

Our *in vivo* experiments revealed that MCAM knockdown in PCa cells reduces their ability to generate lytic lesions upon inoculation into the bone. We found that MCAM knockdown cells and NT control cells displayed similar tumor burden *in vivo* despite showing different cell proliferation rates *in vitro*. This supports the notion that, in the presence of the bone microenvironment, MCAM has a prominent role in modulating the process of bone remodeling and suggests that, in this context, other mechanisms sustain the proliferation of tumor cells. Treatment with an anti-MCAM mAb revealed significant impact on lytic-lesions in the mice bearing PCa cells in the bone. This finding is in line with the results of our *in vivo* experiment with MCAM knockdown. However, administration of anti-MCAM mAb also resulted in lower tumor burden in the intra-osseous model. This might be related to the residual level of MCAM in our knockdown line (approximately 30% knockdown on the protein level) compared to the administered mAb. We showed here that the reduction in MCAM expression is sufficient to influence the expression of the oncogenic driver CRIPTO/TDGF1 (43). This suggests that in MCAM knockdown in PCa cells, the proliferation *in vitro* might be supported by TDGF1. Consistent with this possibility, we have previously shown that TDGF1 knockdown decreases cell proliferation *in vitro* and bone metastases *in vivo* and that TDGF1 mRNA increases upon direct co-culture of human PCa cells with human osteoblasts (17). While MCAM knockdown does not prevent PCa growth in bone, it does impact on the lytic-phenotype. This role of MCAM is supported by our RNA sequencing data and transcriptional analysis on a set of genes that was previously shown to regulate bone metastasis in lytic-PCa cells (41). MCAM knockdown reduces the mRNA of the osteolytic-factor PTHLH (44) and the Wnt inhibitor dickkopf-1 (DKK-1) (45). DKK-1 expression was proposed as an early event in skeletal metastasis thus favouring osteolysis at the metastatic site (45). Additionally, the concurrent downregulation of PTHLH upon MCAM knockdown might explain the effect on cell proliferation measured *in vitro*, given that PTHLH was shown to play a role in PCa cells proliferation (46).

We found that in human PCa patients MCAM is significantly elevated in androgen-ablation resistant metastases relative to primary tumors. This is in line with our findings that MCAM is elevated upon castration. Moreover, this matches previous clinical literature reporting that MCAM expression is strongly related to poor prognosis in a variety of carcinomas including prostate cancer (37).

We have shown that while it is possible to isolate a fraction of MCAM^{high} and MCAM^{low} cells, their molecular features do not necessarily overlap with those of "bulk" ALDH^{high} and ALDH^{low} cells as shown by our clonogenic assay. This suggests that further subpopulations of cells might display independent phenotypic characteristics as we showed here for the MCAM^{high} fraction.
Our findings also suggest that the modulation of MCAM expression might impact on the transcriptional program of EMT related genes. This is in line with previous studies showing that MCAM promotes EMT and EMT-related drug resistance (47). However, our data on protein expression highlight a lack of significant effect on the detection of E-cadherin and vimentin at the protein level, possibly due to residual MCAM protein. Extravasation is one of the feature of EMT and MCAM knockdown PCa cells behaved similarly to control cells when injected into zebrafish. Treatment with DHT and MDV3100 revealed no difference in the response of control and knockdown cells to androgen stimulation or blockade. However, administration of DHT resulted in a strong decrease in MCAM expression compared to castration. This finding and our analysis of two PCa bone metastasis subset of AR driven and non-AR driven disease, supports the involvement of MCAM during disease progression and reinforce the hypothesis of targeting MCAM in advanced disease.
In conclusion, we have analysed the role of MCAM in PCa cells by investigating its biological function with models that recapitulate the presence and absence of androgens and the ostoblastic-niche *in vitro* and the context of the bone microenvironment *in vivo*. Although additional studies are required to dissect the molecular function of MCAM, our data indicate that MCAM is required for producing the lytic-phenotype in PCa bone metastasis. Moreover, we showed here that treatment with anti-MCAM monoclonal antibody has a significant impact on PCa cells growth intra-bone and diminishes the extension of lytic lesions. Our findings affirm the potential utility of MCAM targeting agents that are able to interfere with its biological function for use in treating metastatic disease to the bone. The combination of these agents with currently available drugs that target PCa growth might lead to better treatment for PCa patients, especially those with life-threatening metastatic disease.

Author contributions

EZ, LA, GvdP, GNT and MK designed the study. EZ and LA performed the experiments, analysed the data and wrote the manuscript. JM, JG, LC and IK performed the experiments. PK, KF and ES provided reagents. CKY and SP analysed the RNA sequencing data and helped with the writing of the paper.

Acknowledgements

The authors thank Guido de Roo and Sabrina Veld from the flow cytometry facility (Department of Hematology, LUMC, The Netherlands). We also would like to thank Stefan Müller, Bernadette Nyfeler and Thomas Schaffer from the FACS laboratory (Department of BioMedical Research, UniBern, Switzerland). Monoclonal anti-human MCAM and rat anti-mouse MCAM antibodies were kindly provided by Prothena Biosciences.

References

1. Jemal A, Center MM, DeSantis C, Ward EM. Global patterns of cancer incidence and mortality rates and trends. Cancer Epidemiol Biomarkers Prev **2010**;19(8):1893-907 doi 10.1158/1055-9965.EPI-10-0437.
2. Bolla M, Van Tienhoven G, Warde P, Dubois JB, Mirimanoff RO, Storme G*, et al.* External irradiation with or without long-term androgen suppression for prostate cancer with high metastatic risk: 10-year results of an EORTC randomised study. Lancet Oncol **2010**;11(11):1066-73 doi 10.1016/S1470-2045(10)70223-0.
3. La Manna F, Karkampouna S, Zoni E, De Menna M, Hensel J, Thalmann GN*, et al.* Metastases in Prostate Cancer. Cold Spring Harb Perspect Med **2018** doi 10.1101/cshperspect.a033688.
4. Hensel J, Thalmann GN. Biology of Bone Metastases in Prostate Cancer. Urology **2016**;92:6-13 doi 10.1016/j.urology.2015.12.039.
5. Shiozawa Y, Pedersen EA, Havens AM, Jung Y, Mishra A, Joseph J*, et al.* Human prostate cancer metastases target the hematopoietic stem cell niche to establish footholds in mouse bone marrow. J Clin Invest **2011**;121(4):1298-312 doi 10.1172/JCI43414.
6. Özdemir BC, Hensel J, Secondini C, Wetterwald A, Schwaninger R, Fleischmann A*, et al.* The Molecular Signature of the Stroma Response in Prostate Cancer-Induced Osteoblastic Bone Metastasis Highlights Expansion of Hematopoietic and Prostate Epithelial Stem Cell Niches. PLoS ONE **2014**;9(12):e114530 doi 10.1371/journal.pone.0114530.
7. Sers C, Kirsch K, Rothbacher U, Riethmuller G, Johnson JP. Genomic organization of the melanoma-associated glycoprotein MUC18: implications for the evolution of the immunoglobulin domains. Proceedings of the National Academy of Sciences **1993**;90(18):8514-8 doi 10.1073/pnas.90.18.8514.
8. Wu G-J, Wu M-WH, Wang S-W, Liu Z, Qu P, Peng Q*, et al.* Isolation and characterization of the major form of human MUC18 cDNA gene and correlation of MUC18 over-expression in prostate cancer cell lines and tissues with malignant progression. Gene **2001**;279(1):17-31 doi 10.1016/s0378-1119(01)00736-3.
9. Xie S, Luca M, Huang S, Gutman M, Reich R, Johnson JP*, et al.* Expression of MCAM/MUC18 by human melanoma cells leads to increased tumor growth and metastasis. Cancer Res **1997**;57(11):2295-303.
10. Kristiansen G, Yu Y, Schlüns K, Sers C, Dietel M, Petersen I. Expression of the Cell Adhesion Molecule CD146/MCAM in Non-Small Cell Lung Cancer. Analytical Cellular Pathology **2003**;25(2):77-81 doi 10.1155/2003/574829.
11. Aldovini D, Demichelis F, Doglioni C, Di Vizio D, Galligioni E, Brugnara S*, et al.* M-CAM expression as marker of poor prognosis in epithelial ovarian cancer. International Journal of Cancer **2006**;119(8):1920-6 doi 10.1002/ijc.22082.
12. Zabouo G, Imbert AM, Jacquemier J, Finetti P, Moreau T, Esterni B*, et al.* CD146 expression is associated with a poor prognosis in human breast

tumors and with enhanced motility in breast cancer cell lines. Breast Cancer Res **2009**;11(1):R1 doi 10.1186/bcr2215.
13. Wu G-J, Wu M-WH, Wang C, Liu Y. Enforced Expression of METCAM/MUC18 Increases Tumorigenesis of Human Prostate Cancer LNCaP Cells in Nude Mice. The Journal of Urology **2011**;185(4):1504-12 doi 10.1016/j.juro.2010.11.052.
14. Zeng Q, Li W, Lu D, Wu Z, Duan H, Luo Y*, et al.* CD146, an epithelial-mesenchymal transition inducer, is associated with triple-negative breast cancer. Proceedings of the National Academy of Sciences **2011**;109(4):1127-32 doi 10.1073/pnas.1111053108.
15. Sacchetti B, Funari A, Michienzi S, Di Cesare S, Piersanti S, Saggio I*, et al.* Self-renewing osteoprogenitors in bone marrow sinusoids can organize a hematopoietic microenvironment. Cell **2007**;131(2):324-36 doi 10.1016/j.cell.2007.08.025.
16. Bardin N. Identification of CD146 as a component of the endothelial junction involved in the control of cell-cell cohesion. Blood **2001**;98(13):3677-84 doi 10.1182/blood.v98.13.3677.
17. Zoni E, Chen L, Karkampouna S, Granchi Z, Verhoef EI, La Manna F*, et al.* CRIPTO and its signaling partner GRP78 drive the metastatic phenotype in human osteotropic prostate cancer. Oncogene **2017**;36(33):4739-49 doi 10.1038/onc.2017.87.
18. Zoni E, van der Horst G, van de Merbel AF, Chen L, Rane JK, Pelger RC*, et al.* miR-25 Modulates Invasiveness and Dissemination of Human Prostate Cancer Cells via Regulation of alphav- and alpha6-Integrin Expression. Cancer Res **2015**;75(11):2326-36 doi 10.1158/0008-5472.CAN-14-2155.
19. Kroon J, in 't Veld LS, Buijs JT, Cheung H, van der Horst G, van der Pluijm G. Glycogen synthase kinase-3β inhibition depletes the population of prostate cancer stem/progenitor-like cells and attenuates metastatic growth. Oncotarget **2013**;5(19):8986-94 doi 10.18632/oncotarget.1510.
20. Bassett JH, van der Spek A, Gogakos A, Williams GR. Quantitative X-ray imaging of rodent bone by Faxitron. Methods Mol Biol **2012**;816:499-506 doi 10.1007/978-1-61779-415-5_29.
21. Breuer J, Korpos E, Hannocks MJ, Schneider-Hohendorf T, Song J, Zondler L*, et al.* Blockade of MCAM/CD146 impedes CNS infiltration of T cells over the choroid plexus. J Neuroinflammation **2018**;15(1):236 doi 10.1186/s12974-018-1276-4.
22. Flanagan K, Fitzgerald K, Baker J, Regnstrom K, Gardai S, Bard F*, et al.* Laminin-411 is a vascular ligand for MCAM and facilitates TH17 cell entry into the CNS. PLoS One **2012**;7(7):e40443 doi 10.1371/journal.pone.0040443.
23. Stoletov K, Montel V, Lester RD, Gonias SL, Klemke R. High-resolution imaging of the dynamic tumor cell vascular interface in transparent zebrafish. Proc Natl Acad Sci U S A **2007**;104(44):17406-11 doi 10.1073/pnas.0703446104.
24. Dobin A, Davis CA, Schlesinger F, Drenkow J, Zaleski C, Jha S*, et al.* STAR: ultrafast universal RNA-seq aligner. Bioinformatics **2013**;29(1):15-21 doi 10.1093/bioinformatics/bts635.
25. Wilkerson MD, Hayes DN. ConsensusClusterPlus: a class discovery tool with confidence assessments and item tracking. Bioinformatics **2010**;26(12):1572-3 doi 10.1093/bioinformatics/btq170.

26. Nikolayeva O, Robinson MD. edgeR for differential RNA-seq and ChIP-seq analysis: an application to stem cell biology. Methods Mol Biol **2014**;1150:45-79 doi 10.1007/978-1-4939-0512-6_3.
27. Subramanian A, Tamayo P, Mootha VK, Mukherjee S, Ebert BL, Gillette MA*, et al.* Gene set enrichment analysis: a knowledge-based approach for interpreting genome-wide expression profiles. Proc Natl Acad Sci U S A **2005**;102(43):15545-50 doi 10.1073/pnas.0506580102.
28. Liberzon A, Subramanian A, Pinchback R, Thorvaldsdottir H, Tamayo P, Mesirov JP. Molecular signatures database (MSigDB) 3.0. Bioinformatics **2011**;27(12):1739-40 doi 10.1093/bioinformatics/btr260.
29. Reimand J, Arak T, Adler P, Kolberg L, Reisberg S, Peterson H*, et al.* g:Profiler-a web server for functional interpretation of gene lists (2016 update). Nucleic Acids Res **2016**;44(W1):W83-9 doi 10.1093/nar/gkw199.
30. Shannon P, Markiel A, Ozier O, Baliga NS, Wang JT, Ramage D*, et al.* Cytoscape: a software environment for integrated models of biomolecular interaction networks. Genome Res **2003**;13(11):2498-504 doi 10.1101/gr.1239303.
31. Dumas J, Gargano MA, Dancik GM. shinyGEO: a web-based application for analyzing gene expression omnibus datasets. Bioinformatics **2016**;32(23):3679-81 doi 10.1093/bioinformatics/btw519.
32. Chandran UR, Ma C, Dhir R, Bisceglia M, Lyons-Weiler M, Liang W*, et al.* Gene expression profiles of prostate cancer reveal involvement of multiple molecular pathways in the metastatic process. BMC Cancer **2007**;7:64 doi 10.1186/1471-2407-7-64.
33. Yu YP, Landsittel D, Jing L, Nelson J, Ren B, Liu L*, et al.* Gene expression alterations in prostate cancer predicting tumor aggression and preceding development of malignancy. J Clin Oncol **2004**;22(14):2790-9 doi 10.1200/JCO.2004.05.158.
34. Ylitalo EB, Thysell E, Jernberg E, Lundholm M, Crnalic S, Egevad L*, et al.* Subgroups of Castration-resistant Prostate Cancer Bone Metastases Defined Through an Inverse Relationship Between Androgen Receptor Activity and Immune Response. Eur Urol **2017**;71(5):776-87 doi 10.1016/j.eururo.2016.07.033.
35. Goswami CP, Nakshatri H. PROGgene: gene expression based survival analysis web application for multiple cancers. J Clin Bioinforma **2013**;3(1):22 doi 10.1186/2043-9113-3-22.
36. Gulzar ZG, McKenney JK, Brooks JD. Increased expression of NuSAP in recurrent prostate cancer is mediated by E2F1. Oncogene **2013**;32(1):70-7 doi 10.1038/onc.2012.27.
37. Wu G-J, Varma VA, Wu M-WH, Wang S-W, Qu P, Yang H*, et al.* Expression of a human cell adhesion molecule, MUC18, in prostate cancer cell lines and tissues. The Prostate **2001**;48(4):305-15 doi 10.1002/pros.1111.
38. van den Hoogen C, van der Horst G, Cheung H, Buijs JT, Lippitt JM, Guzman-Ramirez N*, et al.* High Aldehyde Dehydrogenase Activity Identifies Tumor-Initiating and Metastasis-Initiating Cells in Human Prostate Cancer. Cancer Research **2010**;70(12):5163-73 doi 10.1158/0008-5472.can-09-3806.
39. Sedelaar JP, Isaacs JT. Tissue culture media supplemented with 10% fetal calf serum contains a castrate level of testosterone. Prostate **2009**;69(16):1724-9 doi 10.1002/pros.21028.

40. Cai C, He HH, Chen S, Coleman I, Wang H, Fang Z*, et al.* Androgen receptor gene expression in prostate cancer is directly suppressed by the androgen receptor through recruitment of lysine-specific demethylase 1. Cancer Cell **2011**;20(4):457-71 doi 10.1016/j.ccr.2011.09.001.
41. Fournier PG, Juarez P, Jiang G, Clines GA, Niewolna M, Kim HS*, et al.* The TGF-beta Signaling Regulator PMEPA1 Suppresses Prostate Cancer Metastases to Bone. Cancer Cell **2015**;27(6):809-21 doi 10.1016/j.ccell.2015.04.009.
42. Klauzinska M, Castro NP, Rangel MC, Spike BT, Gray PC, Bertolette D*, et al.* The multifaceted role of the embryonic gene Cripto-1 in cancer, stem cells and epithelial-mesenchymal transition. Semin Cancer Biol **2014**;29:51-8 doi 10.1016/j.semcancer.2014.08.003.
43. Terry S, El-Sayed IY, Destouches D, Maille P, Nicolaiew N, Ploussard G*, et al.* CRIPTO overexpression promotes mesenchymal differentiation in prostate carcinoma cells through parallel regulation of AKT and FGFR activities. Oncotarget **2015**;6(14):11994-2008 doi 10.18632/oncotarget.2740.
44. Powell GJ, Southby J, Danks JA, Stillwell RG, Hayman JA, Henderson MA*, et al.* Localization of parathyroid hormone-related protein in breast cancer metastases: increased incidence in bone compared with other sites. Cancer Res **1991**;51(11):3059-61.
45. Hall CL, Kang S, MacDougald OA, Keller ET. Role of Wnts in prostate cancer bone metastases. J Cell Biochem **2006**;97(4):661-72 doi 10.1002/jcb.20735.
46. Asadi F, Faraj M, Malakouti S, Kukreja SC. Effect of parathyroid hormone related protein, and dihydrotestosterone on proliferation and ornithine decarboxylase mRNA in human prostate cancer cell lines. Int Urol Nephrol **2001**;33(3):417-22.
47. Liu WF, Ji SR, Sun JJ, Zhang Y, Liu ZY, Liang AB*, et al.* CD146 expression correlates with epithelial-mesenchymal transition markers and a poor prognosis in gastric cancer. Int J Mol Sci **2012**;13(5):6399-406 doi 10.3390/ijms13056399.

Figure Legends

Figure 1. High expression of MCAM is associated with PCa and PCa metastasis. A-C) MCAM expression in primary normal, primary PCa and tumor adjacent tissue (GSE6919). Expression levels are presented as boxplots. D-E) MCAM expression in primary PCa site compared to distant metastasis in samples from PCa patients (GSE6752). F) Schematic representation of viable cell sorting; a fraction of MCAMHigh and MCAMLow cells (approx. 20% of parental gate) is isolated from the ALDHHigh and from the ALDHLow subpopulation respectively. G) RT-qPCR on the sorted subpopulations for MCAM expression. H-I) Clonogenic assay and quantification of the colony forming capacity of the selected subpopulations after sorting. N=3 technical replicates. Data are presented as mean ± SD. . *p<0.05, **p<0.01; ***p<0.001.

Figure 2. MCAM knockdown in PC-3M-Pro4Luc2dTomato and C4-2BdTomato human PCa cell lines. Functionally active protein expression is evaluated by flowcytometry and displayed panel (A) for PC-3M-Pro4Luc2dTomato cells and (B) for C4-2BdTomato. Data are represented as mean ± SD and are representative of at least 3 independent experiments. **p<0.01; ***p<0.001. C) Evaluation of effect of MCAM knockdown on cell proliferation over 96 hours in PC-3M-Pro4Luc2dTomato cells and control (sh-NT) cells with three independent shRNAs. Data are representative of at least 3 independent experiments. **p<0.01 and ***p<0.001 with Bonferroni Multiple Comparison test. D) Proliferation assay on C4-2BdTomato cells with MCAM knockdown by three independent shRNAs compared to control non-targeted (sh-NT) cells. Data are represented as mean ± SD. ***p<0.001 with Bonferroni Multiple Comparison test. E) ALDEFLUOR assay on MCAM knockdown and non-targeted (NT) PC-3M-Pro4 cells to assess the percentage of ALDHhigh cells upon MCAM knockdown and (F) data quantification. Data are representative of 3 independent experiments and represented as mean ± SD. G) ALDEFLUOR assay on MCAM knockdown and non-targeted (NT) C4-2BdTomato cells to assess the percentage of ALDHhigh cells upon MCAM knockdown and (H) data quantification. Data are representative of 3 independent experiments and represented as mean ± SD.

Figure 3. Effects of MCAM knockdown on EMT markers and characterization of co-culture with human osteoblasts. A-B) MCAM knockdown results in increased ratio E-Cadherin/Vimentin and E-Cadherin/N-Cadherin. Data are representative of 3 independent samples and normalized with housekeeping gene. Data are represented as mean ± SD. C-D) Western blot for E-Cadherin expression and quantification. Calculation is normalized to expression of actin. Data are representative of 3 independent samples. Data are represented as mean ± SD. E-F) Western blot for Vimentin expression, quantification and protein ratio E-Cad/Vim. Calculation is normalized to expression of housekeeping (actin). Data are representative of 3 independent samples. Data are represented as mean ± SD. G) Schematic representation of the co-culture experiment. PC-3M-Pro4 cells expressing dTomato fluorescent protein are cultured in direct contact with differentiated human osteoblasts for 48hrs prior to viable cells sorting. H) Representative images of FACS analysis on ALDH activity on PC3M-Pro4dTomato cells with non-targeted (sh-NT) without osteoblasts (-OB) or with osteoblasts (+OB). Assay was performed immediately after sorting. Same conditions are shown for the MCAM knockdown cells

(2 right panels, figure 3H). In each panel the small insert represents the control used for gating according from manufacturer's protocol. Quantification is displayed in (I). Data are represented as mean ± SEM . **p<0.01 with Bonferroni Multiple Comparison Test.

Figure 4. Expression of MCAM in non-AR driven PCa and in vitro functional effect of DHT treatment. A-B) MCAM and LAMA4 expression in PCa bone metastasis from AR driven and non-AR driven disease (in GSE101607). C) Schematic representation of in vitro castration and AR stimulation. N=3 technical replicates. D) Effect of DHT on AR responsive genes. Results are expressed as the mean ± SD. E) Effect of MDV3100 on AR responsive genes. F) Effect of AR stimulation or inhibition on MCAM expression. Results are expressed as the mean ± SD, * p<0.05, ** p<0.01 and *** p<0.001 with t-test. $$$ p<0.001 between EtOH control and DHT in the respective cell clone.

Figure 5. CB17 SCID male mice inoculated with PC-3M-Pro4Luc2 human PCa cells with non-targeting shRNA (sh-NT) or MCAM-targeting shRNA (shRNA#1) or sham animals. 50.000 cells/animal. See Supplementary information for representation of all the single animals. A, B, C) Representative BLI images and bone measurements with X-Ray (B) and bone morphometric analysis (C). D) Representative histological analysis (H&E staining) of sections of tibia (T, Tumor; B, Bone; BM, Bone Marrow). E) Quantification of the bone area at day 28. Data are represented as mean ± SD. F) Quantification of tumor burden by BLI imaging. G) Expression of genes related to bone metastasis in MCAM KD and non-targeted control (NT) PCa cells. N=3 independent experiments, represented as ± SD. H) Western blot for Cripto expression. Data are representative of 3 independent protein isolations.

Figure 6. RNA sequencing and gene set enrichment analysis. A) Heatmap illustrating hierarchical clustering of the samples, based on the 500 most variable genes and Volcano plot of -log10(p-value) against log2(fold change). Red dots are those with at least 2-fold difference and FDR≤0.05 (i.e. differentially expressed genes). B) GSEA enrichment analysis performed on C5_biological processes. Red bars = up-regulated pathways; Blu bars = downregulated pathways. Numbers on the left (of the blu bars) or on the right (of the red bars) indicate the amount of genes enriched for each gene sets. Data are sorted for NES (x axes). C) GSEA plot for negative regulators of hematopoiesis. Normalized enrichment score (NES) and p-value are indicated in the plot. D) GSEA enrichment plot for biomineral tissue development. E) GSEA enrichment plot for bone mineralization. The plots C-E illustrate profiles of the NES and positions of the genes on the rank ordered list in GSEA. Statistical p-value is also indicated. F) Enrichment map, for C5 (biological processes) displays sets of genes upregulated (red) or downregulated (blue) in MCAM knockdown cells.

Figure 7. CB17 SCID male mice inoculated with PC-3M-Pro4Luc2 human PCa cells intra-bone and treated with anti-MCAM monoclonal antibody. A) Representative BLI images of separate experimental groups (5 animal/group, see supplementary material for representation of all the single animals. 50.000 cells/animal; in the label descriptions of the group names, H = human, M = mouse) B) Quantification of tumor burden by BLI imaging. Data are represented as mean ±

SEM. C) Representative x-ray images of separate experimental groups. See supplementary information for representation of all the single animals. D) Body weight of animals measured over the course of the experiment. Data are represented as mean ± SD. E) Representative images of bone morphometric analysis. See supplementary information for representation of all the single animals and image processing. F) Quantification of the bone area at the end of experiment. Data are represented as mean ± SD. * $p<0.05$ with one way ANOVA and Bonferroni's Multiple Comparison test.

Figure 1

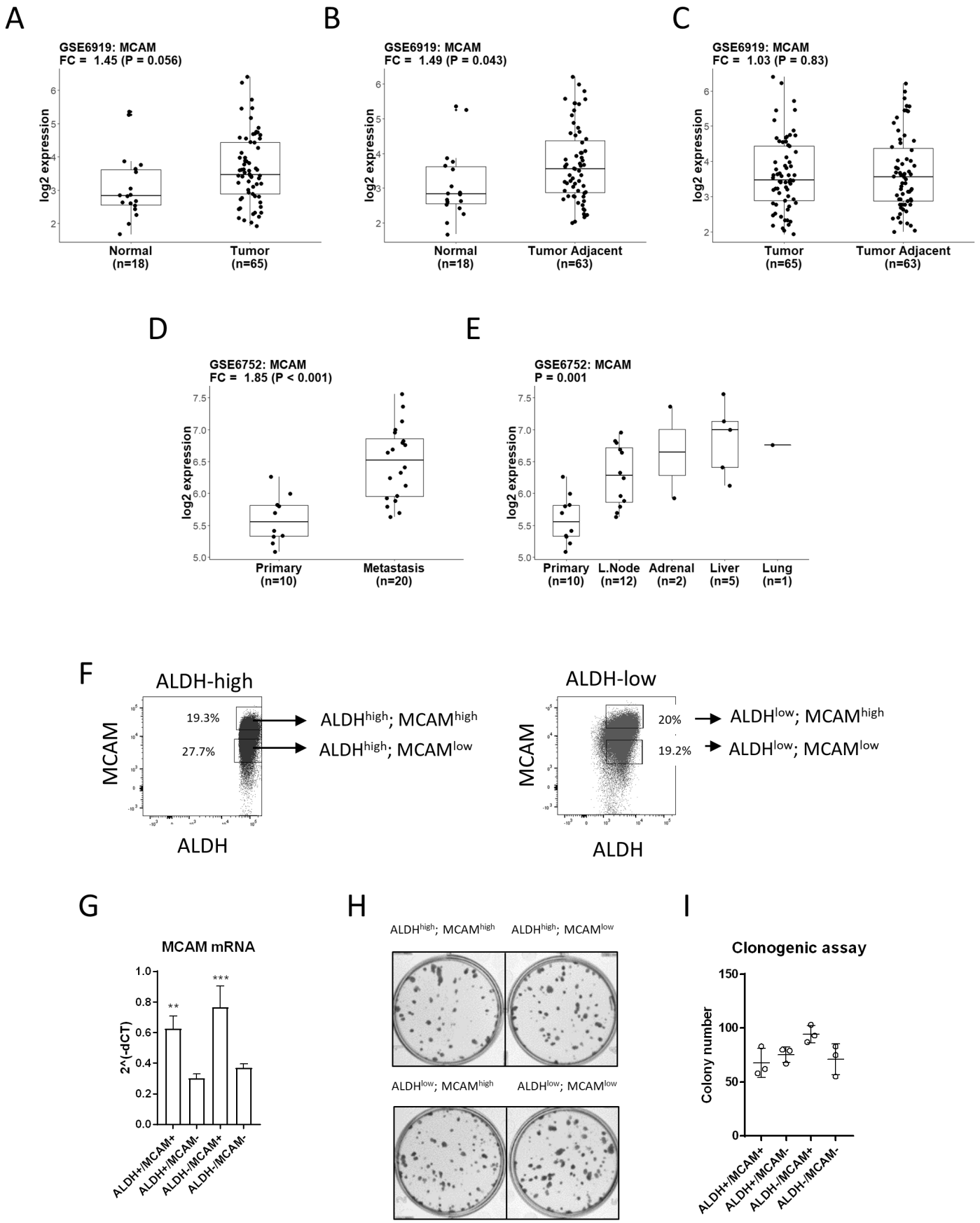
A
GSE6919: MCAM
FC = 1.45 (P = 0.056)
log2 expression
Normal (n=18)
Tumor (n=65)
B
GSE6919: MCAM
FC = 1.49 (P = 0.043)
log2 expression
Normal (n=18)
Tumor Adjacent (n=63)
C
GSE6919: MCAM
FC = 1.03 (P = 0.83)
log2 expression
Tumor (n=65)
Tumor Adjacent (n=63)
D
GSE6752: MCAM
FC = 1.85 (P < 0.001)
log2 expression
Primary (n=10)
Metastasis (n=20)
E
GSE6752: MCAM
P = 0.001
log2 expression
Primary (n=10)
L.Node (n=12)
Adrenal (n=2)
Liver (n=5)
Lung (n=1)
F
ALDH-high
MCAM
ALDH
19.3%
27.7%
ALDHhigh; MCAMhigh
ALDHhigh; MCAMlow
ALDH-low
MCAM
ALDH
20%
19.2%
ALDHlow; MCAMhigh
ALDHlow; MCAMlow
G
MCAM mRNA
2^(-dCT)
**
***
ALDH+/MCAM+
ALDH+/MCAM-
ALDH-/MCAM+
ALDH-/MCAM-
H
ALDHhigh; MCAMhigh
ALDHhigh; MCAMlow
ALDHlow; MCAMhigh
ALDHlow; MCAMlow
I
Clonogenic assay
Colony number
ALDH+/MCAM+
ALDH+/MCAM-
ALDH-/MCAM+
ALDH-/MCAM-

Figure 2

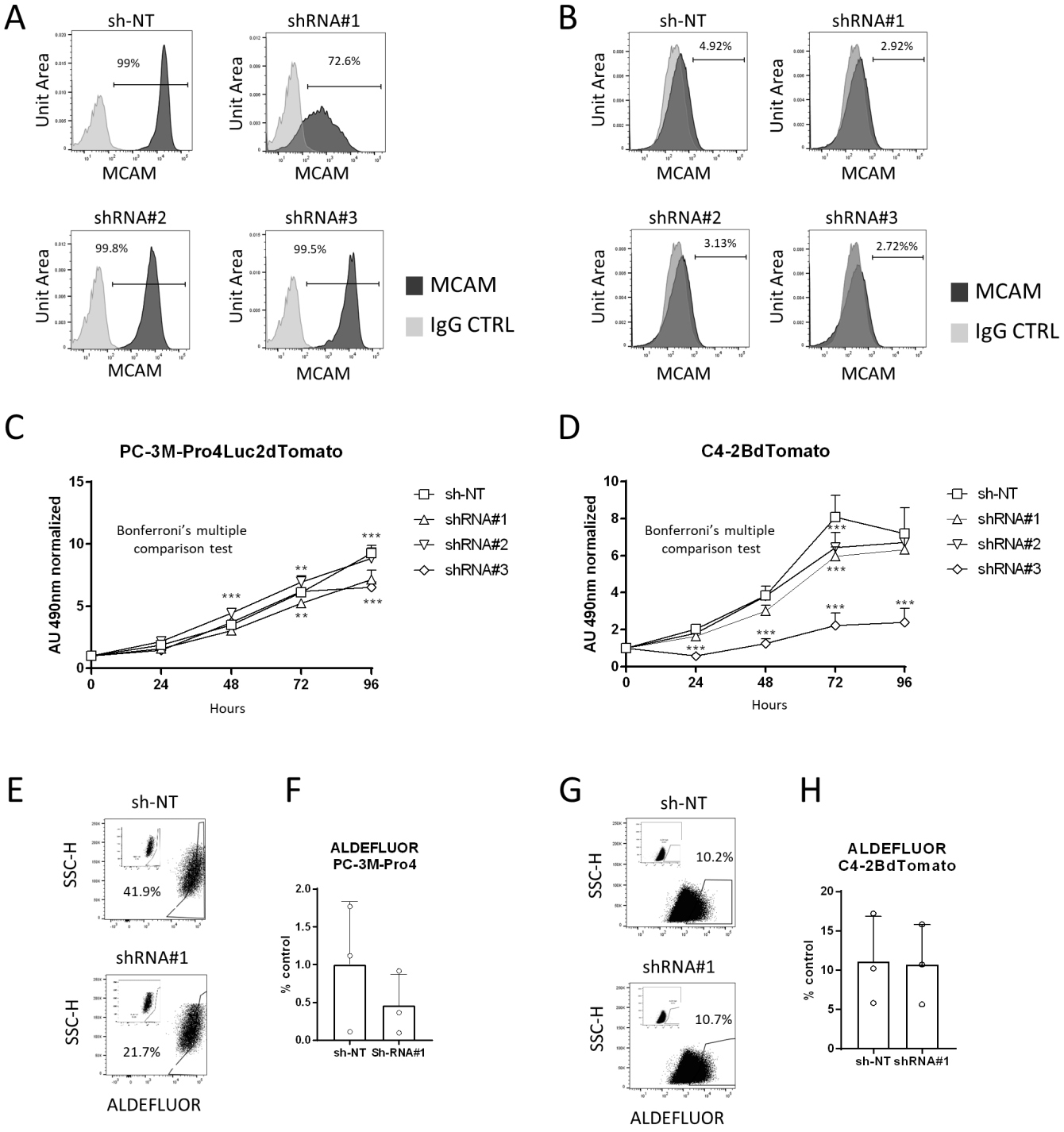
A
sh-NT
shRNA#1
shRNA#2
shRNA#3
Unit Area
MCAM
99%
72.6%
99.8%
99.5%
MCAM
IgG CTRL
B
4.92%
2.92%
3.13%
2.72%%
C
PC-3M-Pro4Luc2dTomato
AU 490nm normalized
Bonferroni's multiple comparison test
Hours
sh-NT
shRNA#1
shRNA#2
shRNA#3
D
C4-2BdTomato
E
SSC-H
41.9%
21.7%
ALDEFLUOR
F
ALDEFLUOR PC-3M-Pro4
% control
sh-NT
Sh-RNA#1
G
10.2%
10.7%
H
ALDEFLUOR C4-2BdTomato
sh-NT
shRNA#1

Figure 3

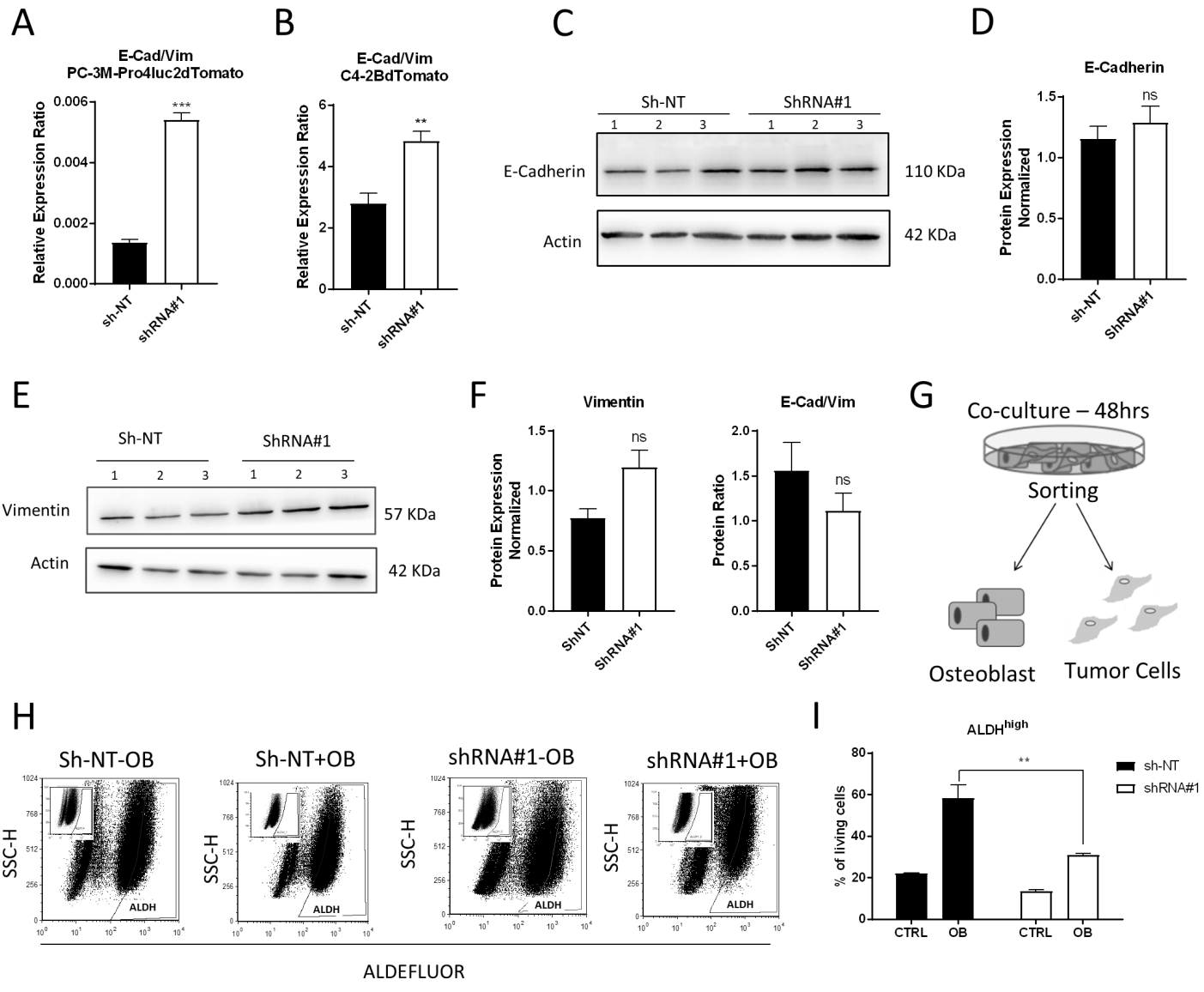
A
E-Cad/Vim
PC-3M-Pro4luc2dTomato
Relative Expression Ratio
0.006
0.004
0.002
0.000
***
sh-NT
shRNA#1
B
E-Cad/Vim
C4-2BdTomato
Relative Expression Ratio
6
4
2
0
**
sh-NT
shRNA#1
C
Sh-NT
ShRNA#1
1 2 3 1 2 3
E-Cadherin
110 KDa
Actin
42 KDa
D
E-Cadherin
Protein Expression Normalized
1.5
1.0
0.5
0.0
ns
sh-NT
ShRNA#1
E
Sh-NT
ShRNA#1
1 2 3 1 2 3
Vimentin
57 KDa
Actin
42 KDa
F
Vimentin
Protein Expression Normalized
1.5
1.0
0.5
0.0
ns
ShNT
ShRNA#1
E-Cad/Vim
Protein Ratio
2.0
1.5
1.0
0.5
0.0
ns
ShNT
ShRNA#1
G
Co-culture – 48hrs
Sorting
Osteoblast
Tumor Cells
H
Sh-NT-OB
Sh-NT+OB
shRNA#1-OB
shRNA#1+OB
SSC-H
ALDH
ALDEFLUOR
I
ALDH^high
% of living cells
80
60
40
20
0
**
sh-NT
shRNA#1
CTRL
OB
CTRL
OB

Figure 4

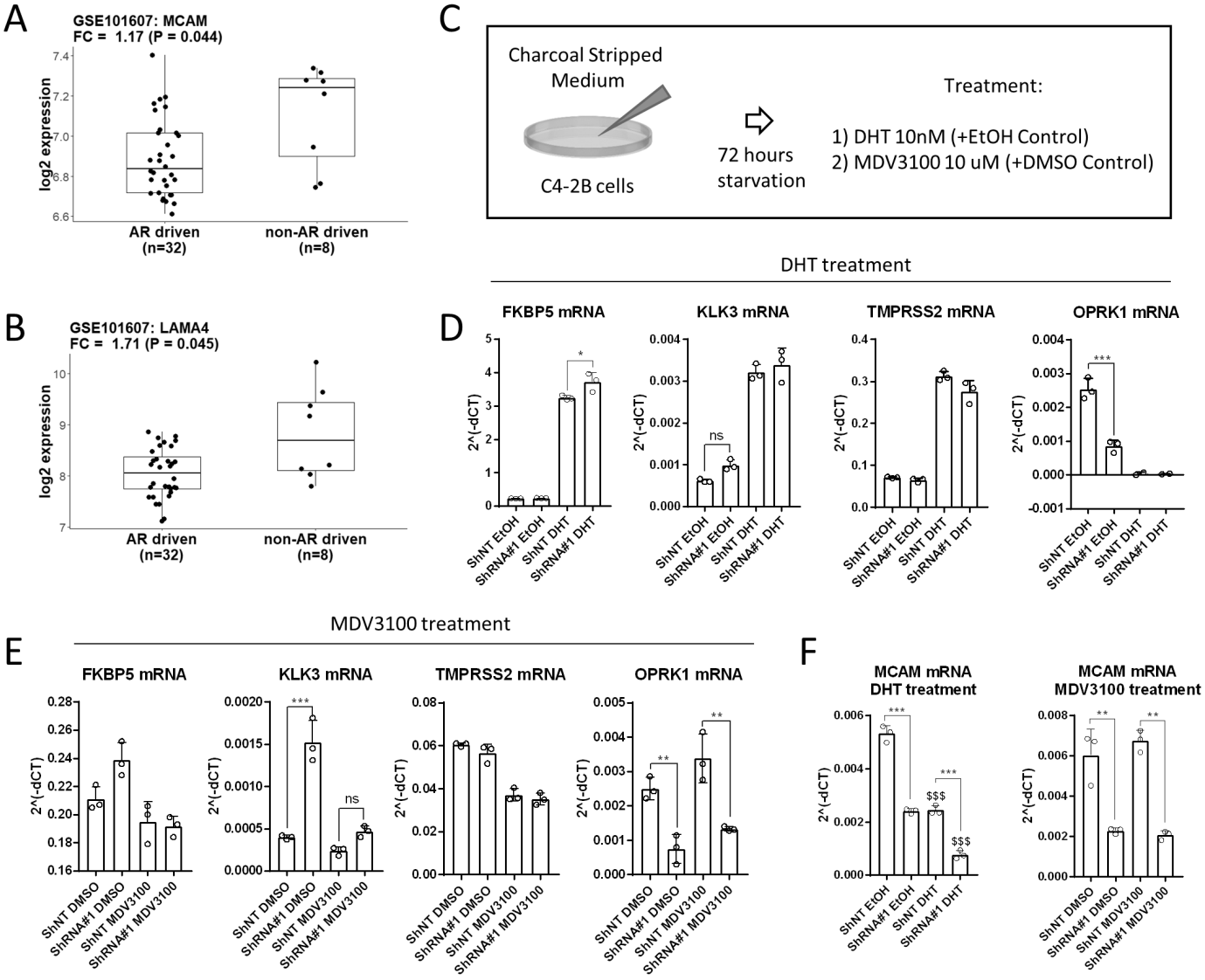
A
GSE101607: MCAM
FC = 1.17 (P = 0.044)
log2 expression
AR driven (n=32)
non-AR driven (n=8)
B
GSE101607: LAMA4
FC = 1.71 (P = 0.045)
log2 expression
AR driven (n=32)
non-AR driven (n=8)
C
Charcoal Stripped Medium
C4-2B cells
72 hours starvation
Treatment:
1) DHT 10nM (+EtOH Control)
2) MDV3100 10 uM (+DMSO Control)
DHT treatment
D
FKBP5 mRNA
KLK3 mRNA
TMPRSS2 mRNA
OPRK1 mRNA
2^(-dCT)
ShNT EtOH
ShRNA#1 EtOH
ShNT DHT
ShRNA#1 DHT
MDV3100 treatment
E
FKBP5 mRNA
KLK3 mRNA
TMPRSS2 mRNA
OPRK1 mRNA
ShNT DMSO
ShRNA#1 DMSO
ShNT MDV3100
ShRNA#1 MDV3100
F
MCAM mRNA DHT treatment
MCAM mRNA MDV3100 treatment

Figure 5

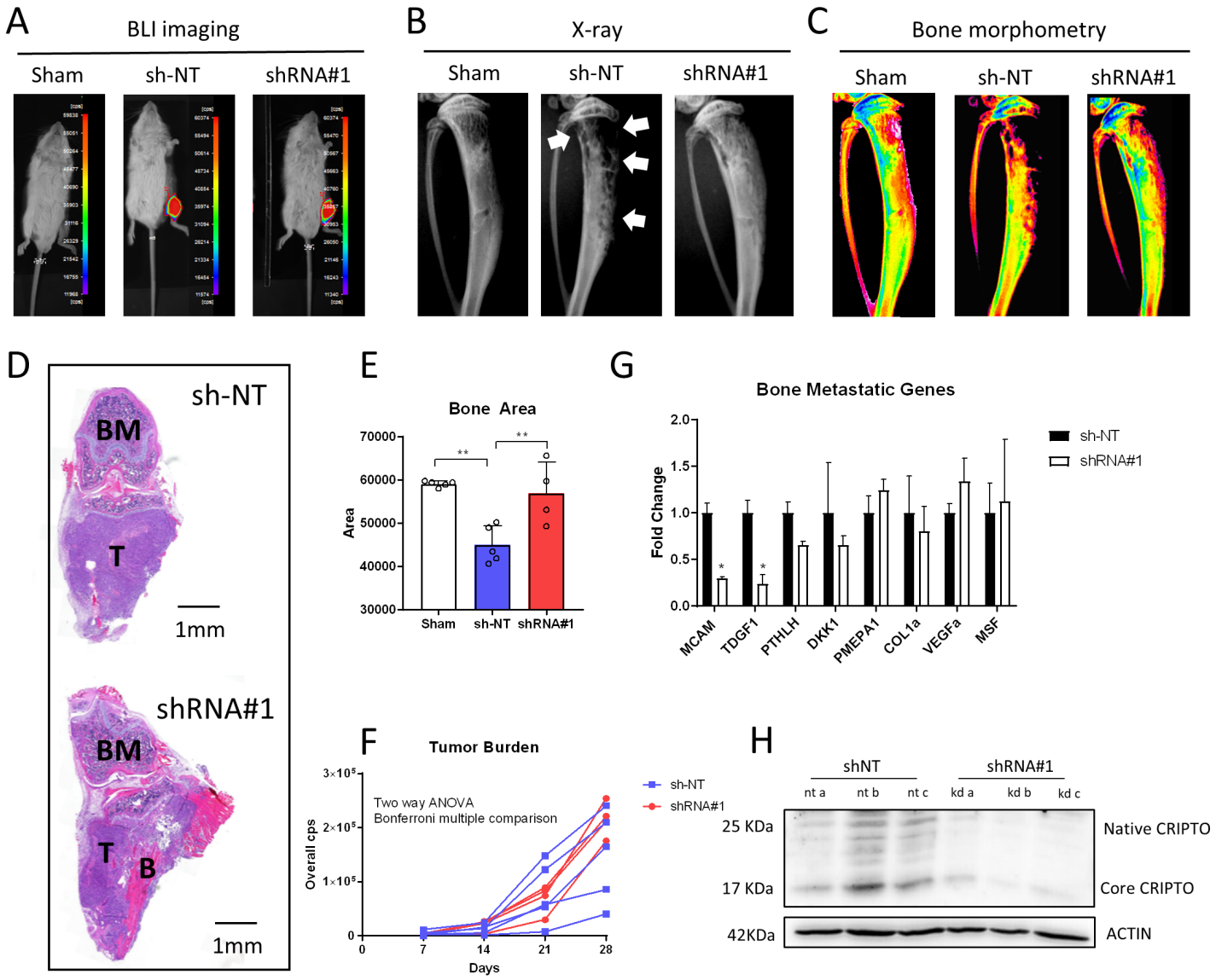
A
BLI imaging
Sham
sh-NT
shRNA#1
B
X-ray
Sham
sh-NT
shRNA#1
C
Bone morphometry
Sham
sh-NT
shRNA#1
D
sh-NT
BM
T
1mm
shRNA#1
BM
T
B
1mm
E
Bone Area
Area
70000
60000
50000
40000
30000
**
**
Sham
sh-NT
shRNA#1
G
Bone Metastatic Genes
Fold Change
2.0
1.5
1.0
0.5
0.0
sh-NT
shRNA#1
MCAM
TDGF1
PTHLH
DKK1
PMEPA1
COL1a
VEGFa
MSF
F
Tumor Burden
Overall cps
3×10⁵
2×10⁵
1×10⁵
0
Two way ANOVA
Bonferroni multiple comparison
0
7
14
21
28
Days
sh-NT
shRNA#1
H
shNT
shRNA#1
nt a
nt b
nt c
kd a
kd b
kd c
25 KDa
17 KDa
42KDa
Native CRIPTO
Core CRIPTO
ACTIN

Figure 6

A

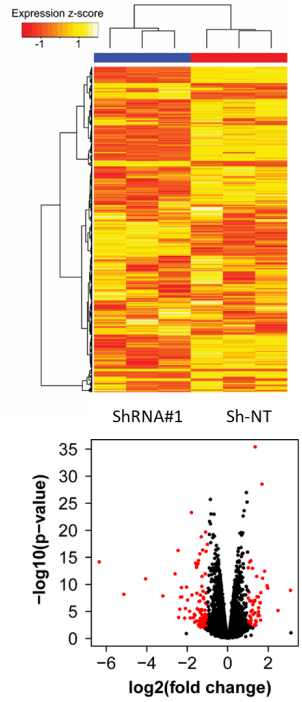

B

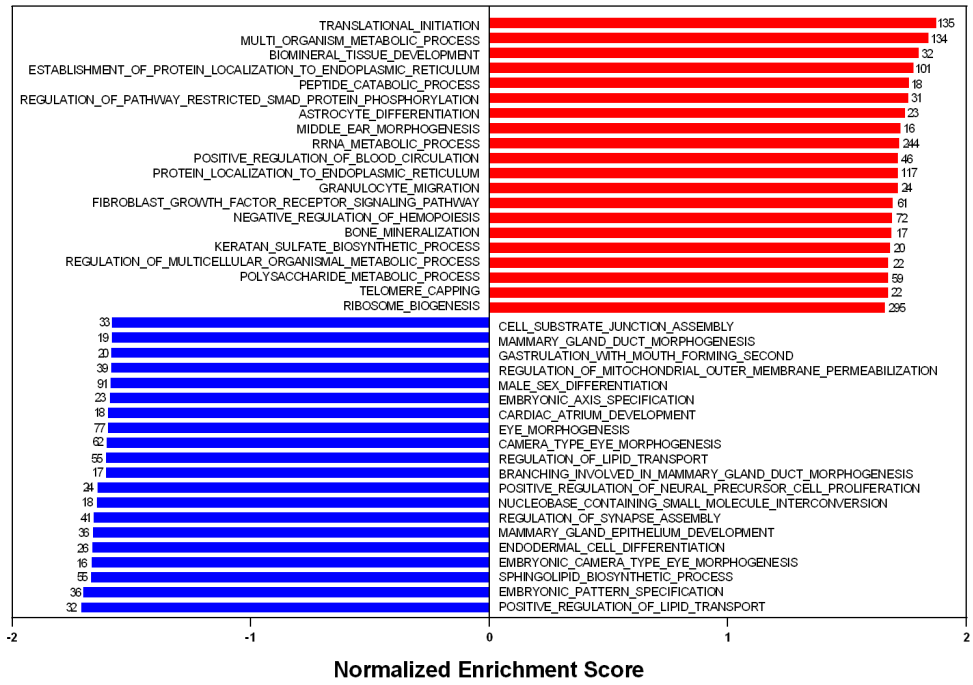

C

GO negative regulation of hemopoiesis

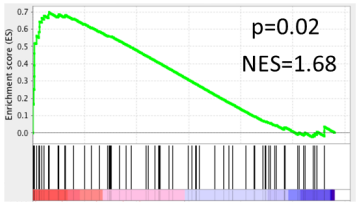

positively correlated — negatively correlated

D

GO biomineral tissue development

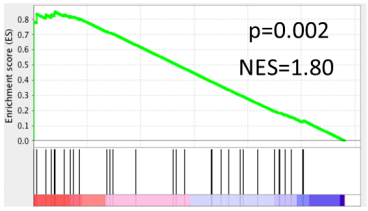

positively correlated — negatively correlated

E

GO bone mineralization

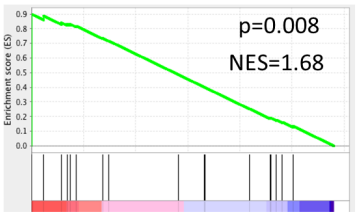

positively correlated — negatively correlated

F

GSEA Enrichment Map

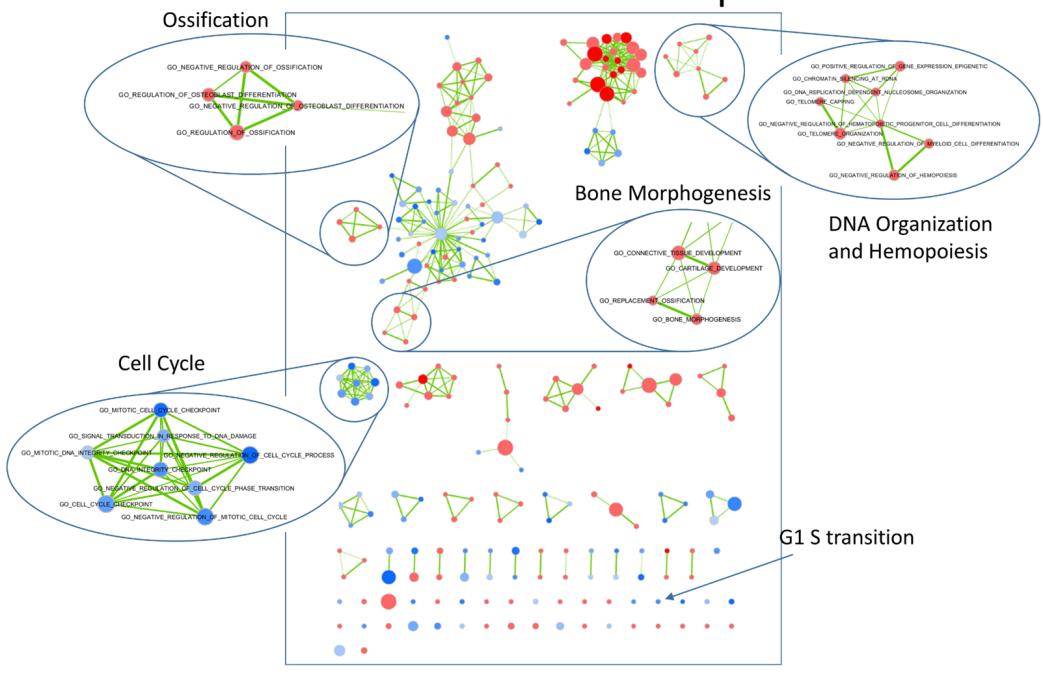

Figure 7

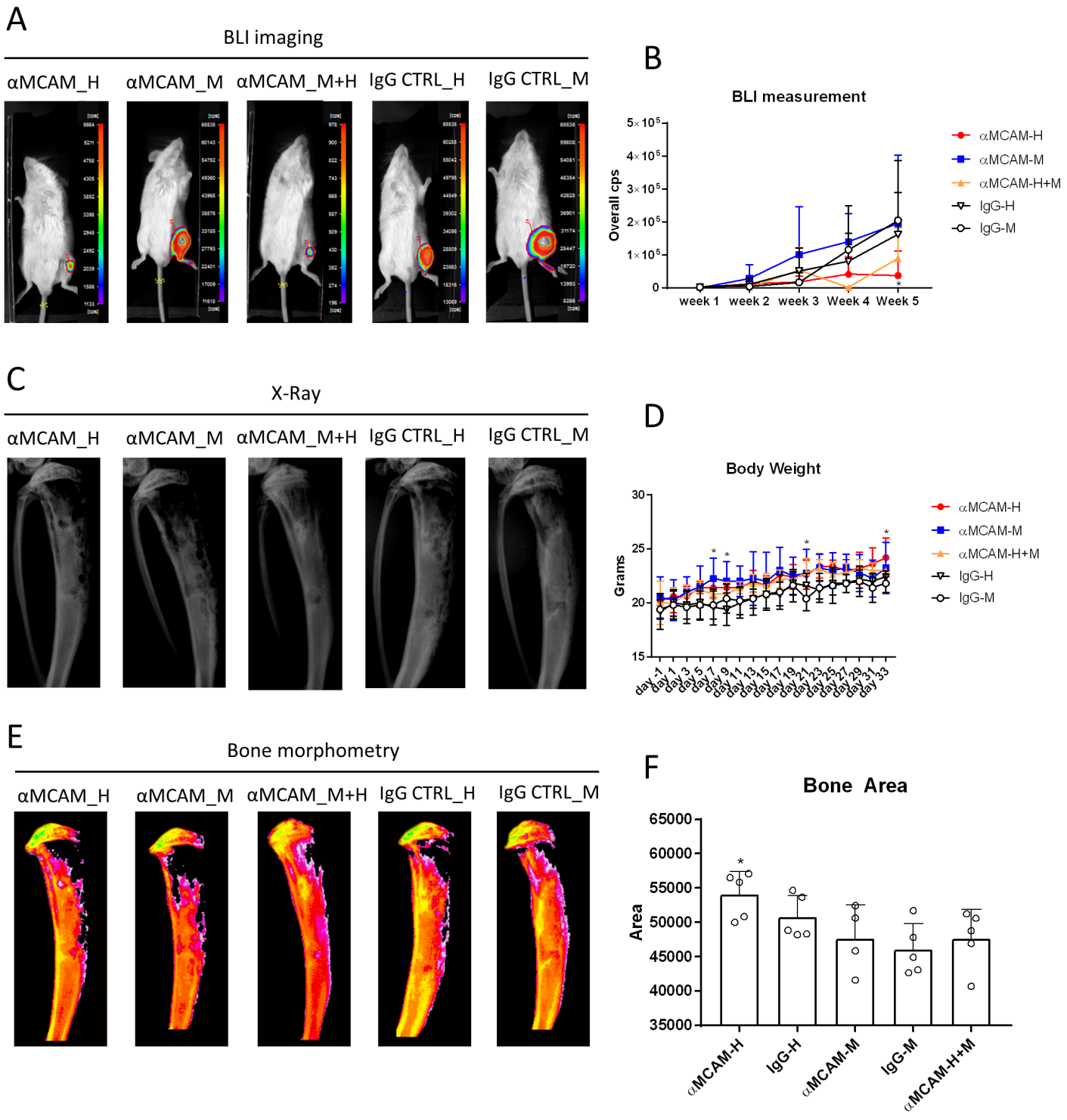
A
BLI imaging
αMCAM_H
αMCAM_M
αMCAM_M+H
IgG CTRL_H
IgG CTRL_M
B
BLI measurement
Overall cps
week 1
week 2
week 3
Week 4
Week 5
αMCAM-H
αMCAM-M
αMCAM-H+M
IgG-H
IgG-M
C
X-Ray
αMCAM_H
αMCAM_M
αMCAM_M+H
IgG CTRL_H
IgG CTRL_M
D
Body Weight
Grams
αMCAM-H
αMCAM-M
αMCAM-H+M
IgG-H
IgG-M
E
Bone morphometry
αMCAM_H
αMCAM_M
αMCAM_M+H
IgG CTRL_H
IgG CTRL_M
F
Bone Area
Area
αMCAM-H
IgG-H
αMCAM-M
IgG-M
αMCAM-H+M